Optimization of Thin Film Composite Polyimide Reverse Osmosis Membrane by Polyethylene Glycol for Enhanced Fouling Resistance

Jyoti Campbell
Chemistry, Wellesley College

NNIN REU Site: Nano Research Facility, Washington University in St. Louis, St. Louis, MO
NNIN REU Principal Investigator: Dr. Young-Shin Jun, Energy, Environmental, and Chemical Engineering, Washington University in St. Louis
NNIN REU Graduate Mentor: Zongsen Zou, Energy, Environmental, and Chemical Engineering, Washington University in St. Louis
Contact: jcampbe5@wellesley.edu, ysjun@wustl.edu, zou.zongsen@wustl.edu

Introduction:

Water scarcity is a serious concern for the world and it is projected to get worse. Water desalination is an important source of fresh water to alleviate water scarcity, especially in water stressed regions, and it will continue to grow in importance. Many desalination plants use reverse osmosis (RO) to generate fresh water [1]. RO is a high pressure process that uses thin film composite polyamide (TFC-PA) membranes to remove contaminants from the water. Unfortunately, these membranes commonly experience fouling, which can decrease water flux and salt rejection [1]. Polyethylene glycol (PEG) is a hydrophilic material that, when attached to the membrane surface, can enhance fouling resistance and increase membrane flux by making the surface both more neutrally charged and hydrophilic [2]. However, multi-component foulant resistance of modified membrane has not been tested. Thus, in this study, we investigated the efficacy of the PEG-modified TFC-PA RO membranes in fouling resistance to calcium carbonate ($CaCO_3$), calcium sulfate ($CaSO_4$), and humic acid.

Experimental Procedure:

One commercially available TFC-PA membrane (BW30) was used to investigate the effect of PEG modification on mineral fouling ($CaSO_4$ and $CaCO_3$) and organic fouling (humic acid). The membrane was soaked in deionized (DI) water for 24 hours before testing or modifying. The membrane was modified in a solution of PEG monomer, PEG crosslinker (ethyleneglycol dimethacrylate), and initiators (potassium persulfate and potassium disulfite). The membrane was then pretreated for membrane compaction and conditioning with DI water for seven hours at 260 psi. Then the membrane was tested with fouling influent for four hours.

There were three fouling influents of interest, all dissolved into DI water. First, $CaCO_3$-forming solution was made by mixing 10 mM NaCl with 3.3 mM $CaCl_2$ and 3.3 mM Na_2CO_3. Second, $CaSO_4$-forming solution was made by mixing 19.5 mM $CaCl_2$, and 19.5 mM Na_2SO_4. Third, humic acid solution was prepared to contain 10 ppm humic acid. Continuous samples of effluent were taken every five minutes. Water flux and salt rejection were tested every five minutes for the first hour, then every 30 minutes. The extent of membrane fouling was examined by contact angle measurement and scanning electron microscopy (SEM).

Results and Discussion:

Before fouling experiments, SEM images showed PEG attached to the modified membrane. Also, contact angle analysis done before fouling showed that PA-PEG had a much lower contact angle at 13.2° than PA at 42.2°.

For fouling experiments, overall, there was less fouling for PA-PEG membranes than for PA membranes. For the $CaCO_3$ fouling experiment, we found the PA and PA-PEG membranes had comparable flux and salt rejection. However, the SEM images show that the PA-PEG membrane has fewer foulants than the PA membrane (Figures 2 and 4). For the $CaSO_4$ fouling experiment, we found that PA-PEG had higher initial flux and Ca^{2+} rejection. However the PA membrane had higher SO_4^{2-} rejection, most likely due to the negative membrane surface having more repulsion with the negatively charged ion than the neutral modified membrane surface. Figure 2 showed no $CaSO_4$ fouling on the PA-PEG membrane, but $CaSO_4$ fouling was present on the PA membrane shown in Figure 1. For the humic acid fouling experiment, PA had higher flux, but based on contact angle showing that the PA surface was more hydrophobic and this should result in a lower flux, this can be an error and should be retested.

The PA-PEG membrane had a higher humic acid and Cl- rejection. It also had a lower contact angle after fouling at 38.3° than the PA membrane after fouling at 55.8° and the SEM image in Figure 4 showed less fouling on the PA-PEG membrane than the PA membrane in Figure 3.

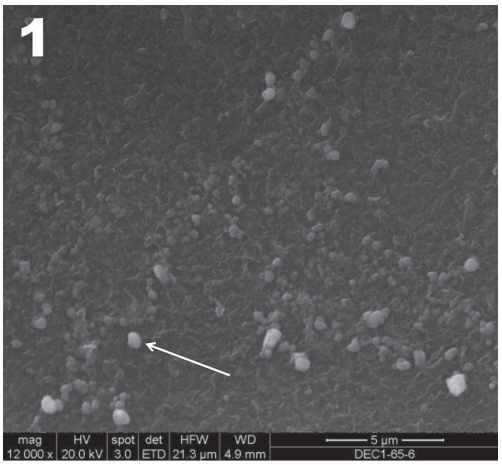

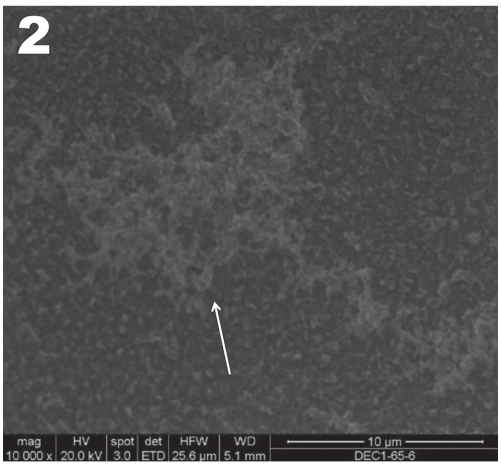

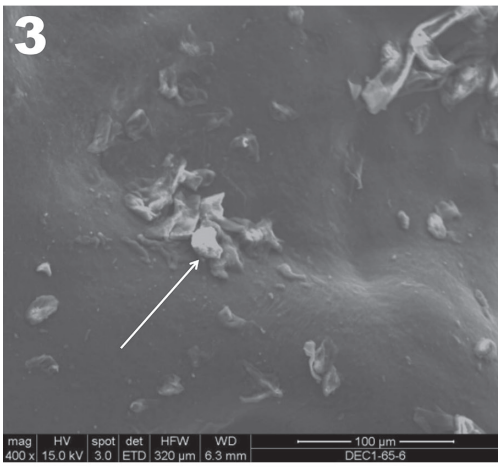

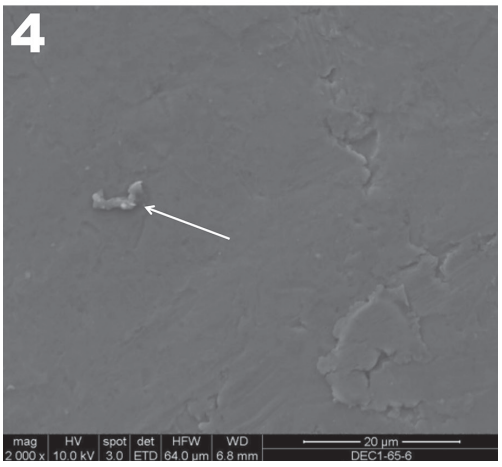

PEG modification makes the PA membrane more hydrophilic resulting in higher initial flux than PA in these experiments. PEG modification of the PA membrane increases fouling resistance to humic acid in particular. Based on contact angle analysis, after humic acid fouling, PA-PEG is still more hydrophilic than PA. At very high mineral foulant concentrations, PEG does not obviously enhance salt rejection, but it enhances resistance to inorganic foulants based on smaller foulant sizes in Figure 2 and SEM images of $CaCO_3$ fouled membranes. More tests should be conducted under different concentrations of foulants.

Conclusions and Future Work:

PEG modification of commercially available TFC-PA membrane makes the surface more hydrophilic which increases initial flux and enhances fouling resistance to humic acid in these fouling experiments. However, at very high mineral foulant concentrations, PEG modification does not obviously enhance salt rejection but does decrease mineral precipitation on the surface. To confirm the trend, replicate experiments are needed. Studies of different influent concentrations, pressures, and combinations should be conducted to determine the impact of PEG modification with realistic and complex influents. In addition, the PEG modification should be further studied and optimized to enhance the fouling resistance of PA RO membranes.

Acknowledgments:

Thank you to Dr. Young-Shin Jun, Mr. Zongsen Zou, Dr. Jessica R. Ray, and everyone at the Environmental Nanochemistry Lab for their guidance and support. I would also like to thank the Nano Research Facility and the National Nanotechnology Infrastructure Network Research Experience for Undergraduates (NNIN REU) Program for giving me this opportunity and unforgettable experience. Support from the National Science Foundation under Grant No. ECCS-0335765, Washington University's International Center for Advanced Renewable Energy & Sustainability (I-CARES).

References:

[1] Menachem Elimelech, William A Phillip. The Future of Seawater Desalination: Energy, Technology, and the Environment [J]. Science 333: 712-717 (2011).

[2] Jessica Ray, et al. Hydrophilic, Bactericidal Nanoheater-Enabled Reverse Osmosis Membranes to Improve Fouling Resistance[J]. ACS Appl. Mater. Interfaces 7(21), 11117-11126 (2015).

__Figure 1__: SEM of PA membrane after $CaSO_4$ fouling test. The white structures are foulant deposits. __Figure 2__: SEM of PA-PEG membrane after $CaSO_4$ fouling test. The white cloud like structures are PEG, not fouling, attached to the membrane surface. __Figure 3__: SEM of PA membrane after humic acid fouling test. The debris on the membrane surface is believed to be humic acid fouling. __Figure 4__: SEM of PA-PEG membrane after humic acid fouling test. The membrane is mostly clear, with one possible smaller foulant.

Twisting a C=C Double Bond in Crowded Alkenes: The Synthesis and Characterization of Small-Molecule Electron Acceptors

Dylan J. Freas
Chemistry, Williams College

NNIN iREU Site: National Institute for Materials Science (NIMS), Tsukuba, Ibaraki, Japan
NNIN iREU Principal Investigator: Dr. Masayuki Takeuchi, Polymer Materials Unit, National Institute for Materials Science
NNIN iREU Mentor: Dr. Atsuro Takai, International Center for Young Scientists, National Institute for Materials Science
Contact: dylan.j.freas@williams.edu, takeuchi.masayuki@nims.go.jp, takai.atsuro@nims.go.jp

Abstract:

There is currently a need for novel, non-fullerene-based electron acceptors in organic photovoltaic devices (OPVs). The synthesis and characterization of various 9,9′-bifluorneylidene (9,9′-BF) derivatives are described. The dihedral angles of the derivatives were determined using DFT calculations and were determined to increase upon introduction of methyl substituents on the inner C1 and C8 atoms. The red shifted UV-vis absorption spectra and negative shift in oxidation potential, determined by cyclic voltammetry, were observed with increasing the C=C dihedral angles of the derivatives. This is, to our knowledge, the first experimental evidence that the degree of C=C bond twisting has profound effects on the bandgap and redox properties of small molecules.

Introduction:

One of the major objectives for materials science is the optimization of the performance of organic photovoltaic devices (OPVs). In such devices, an appropriate combination of donor and acceptor materials is necessary for efficient charge separation and migration. While several research groups have recently reported a wide range of new polymeric donor molecules, there have been fewer reports on new structures of acceptor molecules [1]. Most current acceptor molecules contain fullerene derivatives — however, due to their difficulty in synthesis and purification, along with their weak absorption in the visible region, the synthesis of new and versatile acceptor molecules is urgently required [2].

There is an inherent potential in acceptor molecules based on 9,9′-bifluorenylidene (9,9′-BF), because the one-electron reduction of 9,9′-BF affords a stable radical anion due to steric strain relief and gain in aromaticity to a 14π electron system [3]. The purpose of this study was to synthesize and characterize a series of novel 9,9′-BF derivatives that differ in the twisting angle of the central C=C double bond, but are similar in other electronic properties. The twisting angle of each 9,9′-BF derivative was correlated to its bandgap and redox properties, which were determined by UV-vis spectroscopy and cyclic voltammetry, respectively.

Experimental Section:

Chemicals were purchased from Sigma-Aldrich and used as received without further purification. All dry solvents were freshly distilled under argon prior to use. ^{1}H and ^{13}C NMR measurements were performed in $CDCl_3$ using a JEOL ECS-400 spectrometer. Chemical shifts are expressed in ppm relative to $CHCl_3$ (7.26 ppm for ^{1}H NMR and 77.36 ppm for ^{13}C NMR). Mass spectrometry was performed by a Shimadzu AXIMA-CFR Plus. Computational analysis and graphical representation were carried out with Spartan ’14 software. Optimized equilibrium geometries were obtained with DFT (B3LYP/6-31G** level basis set) calculation. UV-vis spectra were recorded on a JASCO V-670 using CH_2Cl_2 solutions of the 9,9′-BF derivatives in 1 cm quartz cuvettes at 298K. The spectrum of each derivative was then normalized to its maximum absorption (typically 450-500 nm). The electrochemical measurements were carried out with an Eco Chemie AUTOLAB PGSTAT12 potentiostat in a deaerated solvent containing TBAPF6 (0.10 M) as a supporting electrolyte at 298K. A conventional three-electrode cell was used with a glassy carbon working electrode and a platinum wire as a counter electrode. The redox potentials were measured with respect to a reference electrode: $Ag/AgNO_3$ (1.0×10^{-2} M) with TBAPF6 (0.10 M) in acetonitrile. Ferrocene was employed as an external standard.

Results and Discussion:

Compounds **1**, **2**, and **3**, shown in Figure 1, were synthesized via a coupling reaction according to a previous work [1]. The formation of these compounds was confirmed using ^{1}H and ^{13}C NMR, along with mass spectrometry.

Although the introduction of methyl groups was shown to increase the twisting angle, they should not significantly alter the electronics of the 9,9′-BF derivatives because they are very weak electron donors. This is proven by the comparison of the reduction potentials between non-substituted fluorenone (-1.80 V vs. Fc/Fc^+) and 1,4-dimethylfluorenone (-1.89 V vs. Fc/Fc^+). Methyl groups are therefore an ideal substituent to investigate the effect of C=C twisting on bandgap and redox properties.

The UV-vis absorption spectra for compounds **1**, **2**, and **3** are shown in Figure 2. It was observed that as the twisting angle increased, there was a red-shift in the absorption spectra, indicating a decrease in the bandgap energy. Additionally, the degree of red shift was observed to be directly related to the increase in twisting angle. These results suggest that the bandgap of 9,9′-BF derivatives can be selectively tuned by modifying the twisting angle.

To investigate the redox properties of the derivatives, cyclic voltammetry was performed, shown in Figure 3. Each HOMO-LUMO bandgap of the derivatives was determined from the oxidation and the reduction potentials, E_{ox}-E_{red}. There was a significant decrease in the HOMO-LUMO bandgaps of the derivatives upon an increase in twist angle (from 2.50 eV for compound **1** to 2.27 eV for compound **3**). This result clearly indicates that the C=C twisting angle of the 9,9′-BF derivatives affects the redox potentials, which is fairly consistent with the UV-vis absorption change.

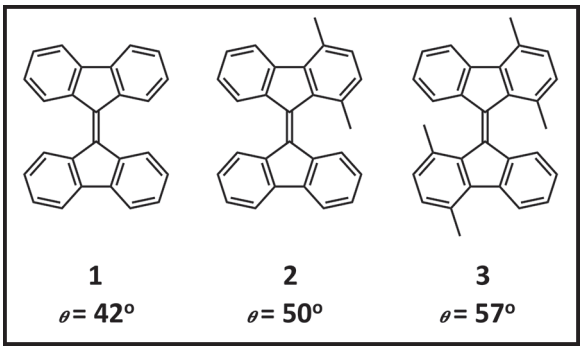

*Figure 1: Structures and C=C double bond twisting angles of compounds **1**, **2**, and **3**.*

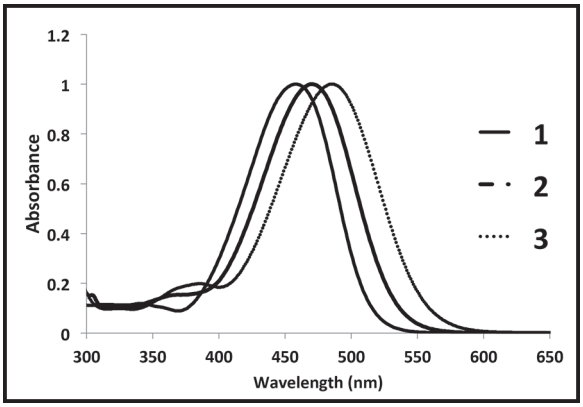

*Figure 2: UV-vis absorption spectra of compounds **1**, **2**, and **3**.*

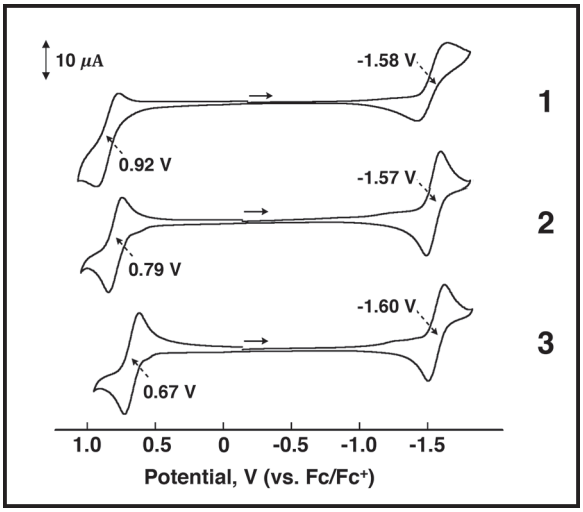

*Figure 3: Cyclic voltammograms of compounds **1**, **2**, and **3**.*

Conclusions and Future Directions:

We showed the synthesis and characterization of a series of new 9,9′-bifluorenylidene derivatives. The central C=C twist angle was correlated to the bandgap and redox properties of the 9,9-BF derivatives. Future work will involve performing x-ray crystallography on the 9,9′-BF derivatives to accurately determine C=C twisting angles. Additionally, the versatile synthetic scheme established in this work will be applied to the synthesis of other 9,9′-BF derivatives that have even greater C=C twisting angles, such as derivatives with $-Si(CH_3)_3$ substituents.

Acknowledgements:

It's very sad to conclude my time with NNIN! Many thanks to my PI, Dr. Masayuki Takeuchi, my mentor, Dr. Atsuro Takai, and the National Nanotechnology Infrastructure Network International Research Experience for Undergraduates (NNIN iREU) Program (Grant No. ECCS-0335765).

References:

[1] Brunetti, et al. Angew. Chem. Int. Ed., 2010, 49, 532-536.

[2] Eakins, et al. Can. J. Chem., 2013, 91, 1059-1071.

[3] Kim, et al. Chem. Comm., 2013, 49, 10950-10952.

Crumpled Graphene Oxide-Polysulfone Composite Membranes for Water Purification

Isaac Fuhrman
Mechanical Engineering, University of Nebraska-Lincoln

NNIN REU Site: Nano Research Facility, Washington University in St. Louis, St. Louis, MO
NNIN REU Principal Investigator: Dr. John Fortner, Energy, Environmental and Chemical Engineering, Washington University in St. Louis
NNIN REU Mentor: Yi Jiang, Energy, Environmental and Chemical Engineering, Washington University in St. Louis
Contact: isaacokoboji@gmail.com, jfortner@wustl.edu, jiang.y@wustl.edu

Abstract:

Previously, crumpled graphene oxide (CGO) has been layered on surfaces of commercial water treatment membranes to increase water flux as well as antimicrobial (anti-biofouling) properties. This study explored CGO's effects on flux, rejection, fouling, and antifouling properties when structurally incorporated into polysulfone (PSF) membranes. Different ratios of CGO were added into the casting solution for a phase-inversion process. The synthesized membranes were then tested in an effort to optimize CGO mass loadings. Proper methods and variables were found and accounted for throughout the series of experiments. Flux and rejection were found as high as 100 L/m² h bar and 90% of BSA respectively. It was hypothesized that surface openings from CGO could serve as water channels through the selective surface toward the more porous region of the membrane, creating higher flux.

Introduction:

Current water treatment methods employ hollow-fiber ultrafiltration (UF) membranes in vast quantities to filter macromolecular impurities and bacteria from feed water for various industrial and residential applications. These modules of membranes require expensive and time-consuming cleaning processes, such as backwashing, in order to remove residue buildup on membrane surfaces. Given the hydrophilic properties of graphene oxide (GO), some research for advancements in water treatment membranes has been geared towards GO nanoparticles.

Previous research has shown that crumpled graphene oxide (CGO) structures can increase flux due to its hydrophilic properties and porous nature [1]. In this study, the effects on polysulfone membrane properties were investigated extensively to determine the performance of CGO as a nanofiller to membrane casting solutions prior to solidification.

Experimental:

Membranes were created using the phase-inversion method [2]. CGO (5-10 mg) was sonicated in n-methyl-2-pyrrolidone (NMP), then stirred with polysulfone (PSF) and polyvinylpyrrolidone (PVP) at 60°C until becoming homogenous. The solution was cast using a casting knife and then submerged in MilliQ water overnight. Subsequently, 63 mm diameter membranes were cut with razor blades.

Transmission electron microscopy (TEM, Tecnai TM Spirit) was utilized to obtain information on CGO and CGO nanocomposites' size and morphologies. Scanning electron microscopy (SEM) images of the membranes (sputtered with Au for 60 s) were taken to examine surface structure.

Membranes were then tested for flux by filtering pure water with a stirred cell under 1.5 bar (Amicon 8200) and measuring permeate weight over 60 s time intervals. Membranes were compacted under 1.5 bar for one hour before any measurement. Water was filtered through the membrane until flux plateaued. Bovine serum albumin (BSA) (1 g/L) was filtered separately as a model foulant. Rejection was determined by the difference between inflow and permeate BSA concentrations that were analyzed at 278 nm using UV-visible spectrophotometry (UV-Vis). All samples were washed with water for several minutes before storing in pure water. Filtration processes were repeated to obtain consistent data as well as fouling and antifouling properties.

Results and Conclusions:

SEM and TEM images in Figure 1 and Figure 2 of CGO membranes show embedded CGO particles directly underneath and protruding from the surface of the membrane. Pristine (control) membranes showed smooth surfaces without notable inconsistencies, forming a smooth solid barrier. CGO nanoparticles channel water from the surface directly into the porous region of the membrane. These particles could be acting as hydrophilic pathways with lower resistance and higher localized flux

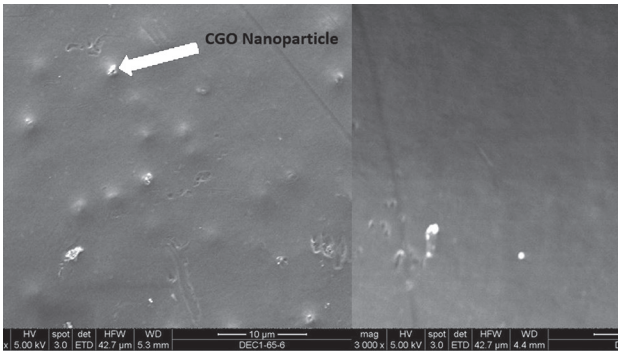

Figure 1: SEM images of CGO nanoparticles protruding through surface of CGO membrane (left) and surface of pristine membrane (right).

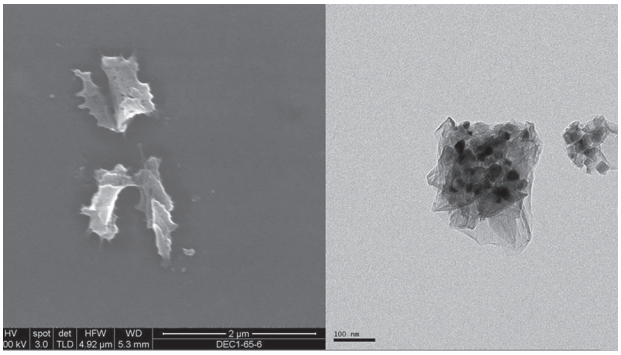

Figure 2: SEM of embedded CGO particle (left) and TEM of CGO with titanium and $CuCl_2$ from aerosolized process [3] (right).

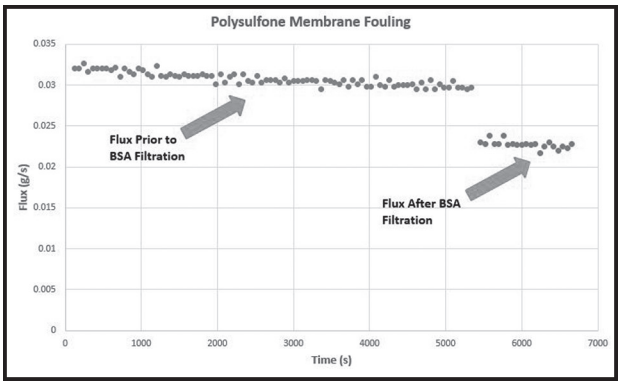

Figure 3: Control membrane fouling before and after BSA filtration.

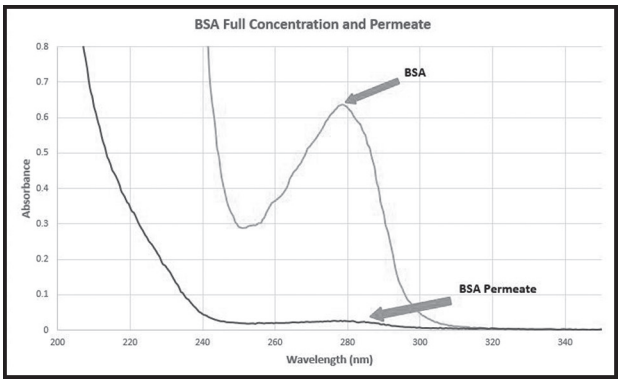

Figure 4: UV-Vis spectrum for inflow BSA and permeate used to determine rejection.

than the surrounding surface, resulting in larger overall flux than membranes without such channels.

Figure 3 shows the fouling process for a pristine membrane. Water flux was found to plateau until a constant value of 0.0295 g/s was reached. After BSA was filtered through the membrane, water flux decreased to 0.0226 g/s — 76.6% of the initial value. Foulant built up on the membrane surface, obstructing pores and decreasing flux. Despite a washing process, not all foulant was removed, damaging the membrane and resulting in a permanently lower flux. This pattern was consistent for both control and CGO membranes alike.

During UV-Vis tests for BSA, absorbance peaked at a wavelength of 278 nm. The linear relationship between concentration and absorbance was compared with the BSA permeate absorbance of each membrane to obtain the remaining BSA in the permeate. An example of a control membrane is given in Figure 4, which has the inflow solution peaking at 0.616 and the permeate at 0.0238, indicating a 96.1% rejection for the given filtration trial.

Rejection for control and CGO membranes ranged from 73.9-96.1% and 70.9-99.2%, respectively, while flux ranged from 0.0176-0.0307 g/s and 0.0155-0.0317 g/s, respectively. Methods to measure both fouling and rejection were refined and will be used for future experiments. Though no statistical differences between CGO and control membranes were found, our preliminary results give base data and processes that will be built further upon by continued research.

Future Work:

The largest issue with results was variability within casting solutions. In future studies the focus should be on consistency and repeatability at each step of experimental processes. Strong evidence was found to support that without the drying process, membranes had up to 10 times higher water flux than dried samples of the same composition, but with a drop of rejection as low as much as 50%. This relationship should be investigated to obtain optimum performance.

Acknowledgements:

I would like to thank my mentor Yi Jiang and PI Dr. John Fortner for the guidance and opportunity to work with them on this project. I would also like to thank NNIN REU and NSF under Grant No. ECCS-0335765.

References:

[1] Jiang, Y, et al., Environ.Sci.& Tech., 49(11), 6846-6854 (2015).

[2] Kim, J, Lee, Y, J.of Membrane Science, 128(2) 153-163 (1998).

[3] Wang, W, Jiang, Y, Biswas, P, The Journal of Physical Chemistry Letters, 3(21), 3228-3233 (2012).

Advanced Dielectrics for Microelectronics: Chemically Amplified, Low-κ Materials

Masashi Fukuzawa
Applied Chemistry, Kyushu University, Fukuoka, Japan

NNIN iREG Site: Institute for Electronics and Nanotechnology, Georgia Institute of Technology, Atlanta, GA
NNIN iREG Principal Investigator: Prof. Paul A. Kohl, Chemical and Biomolecular Engineering, Georgia Institute of Technology
NNIN iREG Mentor: Jared M. Schwartz, Chemical and Biomolecular Engineering, Georgia Institute of Technology
Contact: m.fukuzawa@mail.cstm.kyushu-u.ac.jp, paul.kohl@chbe.gatech.edu, jschwartz38@gatech.edu

Abstract and Introduction:

Shrinking of the microelectronics package requires advanced low dielectric constant (low-κ) materials. Organic polymers offer more environmentally friendly and moldable options than inorganic materials.

In organic polymers, photo-definable dielectrics can be directly patterned by photolithographic means [1]. Lithographically printed dielectrics do not require the use of photoresist or additional pattern transfer steps, which can be costly and expose the device to aggressive wet or dry etch process steps. Some organic, photo-definable polymers can be catalytically depolymerized by a small light stimulus.

The catalytic phenomenon is called chemical amplification, and the polymers that depolymerize completely are called self-immolative polymers (SIPs) [2]. Photo-definable SIPs are depolymerized and become monomers through the light stimulus. Here, if vapor pressure of the monomer is high, the exposed material can evaporate and disappear completely, which can skip the developing steps in traditional processing because only light exposure and dry developing are needed. However, a conventional photo-definable SIP such as polyphthalaldehyde [3] has inherent problems, for example, low mechanical strength and low vapor pressure of monomers.

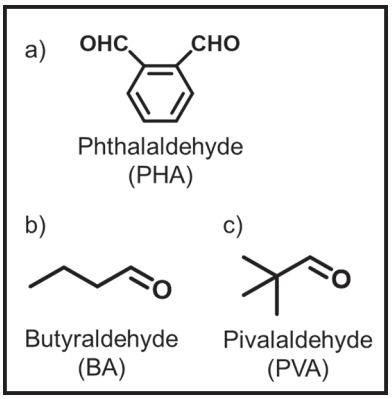

Figure 1: Chemical structures of a) phthalaldehyde (PHA), b) butyraldehyde (BA), and c) pivalaldehyde (PVA).

Low mechanical strength makes them difficult to use as an interlayer insulating film, and low vapor pressure increases dry develop time.

In this report, the preparation method of copolymers that have high mechanical strength and higher vapor pressure is discussed. In order to obtain the ideal copolymer, butyraldehyde (BA) or pivalaldehyde (PVA) are used as a monomer with PHA. BA and PVA has high vapor pressure and their polymers are expected to have high mechanical strength because of their high crystallinity.

Experimental:

Figure 1 shows the monomers used in this research. Copolymers were synthesized by following a paper that describes the anionic polymerization of polyphthalaldehyde [4]. Scheme 1 shows the synthesis procedure of copolymers. PHA (1.0 equiv), BA or PVA (0.25 equiv), and *N*-hydroxysuccinimide in THF (0.01 M, 0.00024 equiv) were added to a vial in a glovebox under an argon atmosphere. THF was added to create a 1.0 M aldehyde solution. The reaction mixture was cooled to -70°C.

After 30 min, a solution of 1-*tert*-butyl-2,2,4,4,4-pentakis(dimethylamino)-2λ^5,4λ^5-catenadi-(phosphazene) (P2-*t*-Bu base) in THF (2.0 M, 0.0048 equiv) was added to the solution, and the reaction mixture was stirred at -70°C. After two hours, the polymer was end-capped via sequential addition of pyridine (0.6 equiv) and methylchloroformate (0.04 equiv) to the -70°C solution. The solution was allowed to warm to room

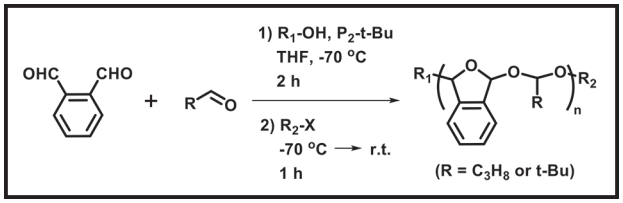

Scheme 1: Synthesis procedure of copolymer.

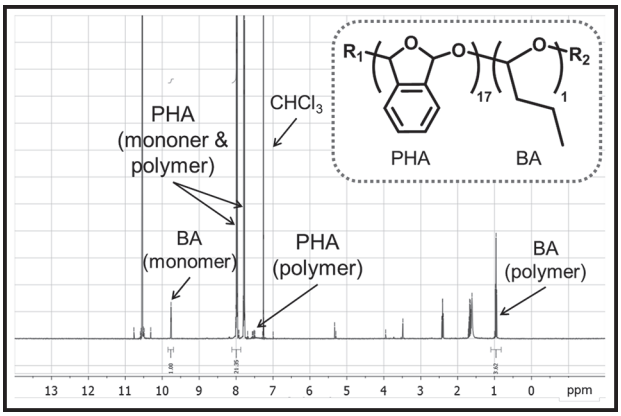

Figure 2: [1]H NMR spectrum of PHA-BA copolymer.

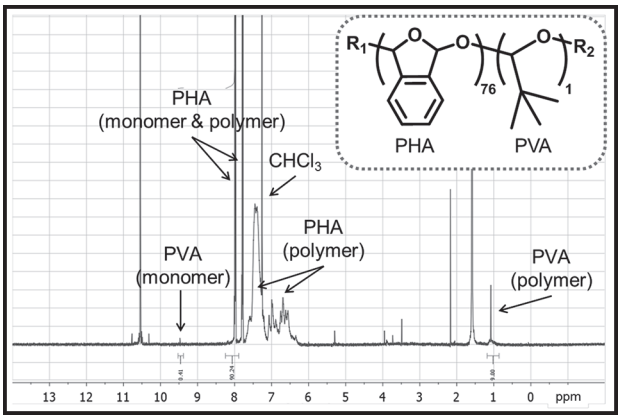

Figure 3: [1]H NMR spectrum of PHA-PVA copolymer.

temperature an hour later. The polymer was precipitated by adding the reaction mixture to a solution of 200 mL cold methanol. The resulting suspension was filtered, and the precipitate was washed using methanol. The resulting polymer was dried overnight.

The yields of the PHA-BA and PHA-PVA copolymers were 42 wt% and 20 wt%, respectively.

Results and Discussion:

Figure 2 shows ^{1}H NMR spectrum of the copolymer, which suggests the mole ratio of PHA to BA is 17 to 1. It suggests the synthesis did not go as expected because the mole ratio was initially 4 to 1. One possible explanation is the acidic α-hydrogens of BA caused a side reaction with the anionic propagation that impeded the polymerization. A copolymer of PHA and PVA was then tried, which has no α-hydrogens to interrupt the polymerization. Figure 3 shows ^{1}H NMR spectrum of the PHA-PVA copolymer, which suggests the ratio of PHA to PVA is 76 to 1. This means almost all of the monomers in the polymer chain are PHA, which is not desired. The low PVA content is probably due to the methyl groups of PVA having high steric hindrance. A new monomer whose methyl groups are substituted for less bulky groups such as fluorine should be used in the future.

Conclusions and Future Work:

A PHA-BA copolymer was synthesized with the goal of obtaining a copolymer with high mechanical strength and high vapor pressure of the monomers. ^{1}H NMR of the copolymer shows the mole ratio of PHA to BA is 17 to 1, which does not substantially improve the monomer vapor pressure after depolymerization as desired. The differences between expected and actual copolymer content is likely due to the α-hydrogens of BA. A PHA-PVA copolymer, which has no α-hydrogens, was attempted, but ^{1}H NMR showed only small amounts of PVA were polymerized. The bulky methyl groups of PVA likely prevented incorporation into the polymer chain. A less bulky monomer that has no α-hydrogens, like 2,2,2-trifluoroacetaldehyde, will be investigated in the future.

Acknowledgements:

This research was supported by the National Nanotechnology Infrastructure Network International Research Experience for Graduates (NNIN iREG) Program and the National Science Foundation (NSF) under Grant No. ECCS-0335765, and the National Institute for Material Science (NIMS). I would like to thank the Dr. Kohl Lab for their valuable guidance and assistance, and Institute for Electronics & Nanotechnology at the Georgia Institute of Technology for providing the equipment and training necessary for this project.

References:

[1] K. Fujikawa, et al., Polym. J. 2008, 40, 281.

[2] A. J. Boydston, et al., Macromolecules 2012, 45, 7317.

[3] S. T. Phillips, et al., J. Am. Chem. Soc. 2010, 132, 9234.

[4] S. T. Phillips, et al., Macromolecules 2013, 46, 2963.

Surface Adsorption and Enzymatic Hydrolysis of Polyphosphates: Implications for Understanding Phosphorus Cycling

Margot Hultz

Materials Science and Engineering, The Johns Hopkins University

NNIN REU Site: Institute for Electronics and Nanotechnology, Georgia Institute of Technology, Atlanta, GA

NNIN REU Principal Investigator: Yuanzhi Tang, Earth and Atmospheric Sciences, Georgia Institute of Technology

NNIN REU Mentor: Rixiang Huang, Earth and Atmospheric Sciences, Georgia Institute of Technology

Contact: mhultz1@jhu.edu, yuanzhi.tang@eas.gatech.edu, rixiang.huang@eas.gatech.edu

Abstract:

Phosphorus (P) is a key, yet often limited, nutrient in aquatic environments. Among various species of P, polyphosphate (polyP) constitutes a significant portion of total P in aquatic environments [1]. PolyP is a polymer of phosphate ions joined by phosphoanhydride (P-O-P) bonds of variable chain length ranging from a few to thousands of phosphate units. It is mainly synthesized by bacteria and plankton. Synthesis of polyP by bacteria is exploited in enhanced biological phosphorus removal (EBPR), a process used to remove excess phosphorus during sewage water treatment. Despite its environmental significance, little is known of the transport, transformation, and fate of polyP.

The goal of this project was to characterize the chemical reactions that may control the transport and stability of polyP in order to understand the larger scale P cycling. Adsorption of polyP onto iron and aluminum oxides was studied using quartz crystal microbalance with dissipation (QCM-D). PolyP hydrolysis catalyzed by alkaline phosphatase was studied by monitoring orthophosphate (orthoP) formation using UV-Vis spectroscopy. It was observed that polyphosphate can be degraded through enzyme-catalyzed hydrolysis with the rate and extent dependent on chain length. In the presence of calcium, precipitation of calcium-phosphate (Ca-P) solid phase(s) was monitored by dynamic light scattering, and the precipitates were characterized using scanning electron microscopy with energy dispersive spectroscopy (SEM-EDX), and Fourier transform infrared spectroscopy (FT-IR). FT-IR spectra and elemental analysis from EDX suggested the precipitate to be a non-apatite phase, likely a type of amorphous Ca-P.

Experimental Procedures:

Total Dissolved Phosphate Assay. Determination of total phosphate in solution was done according to the colorimetric protocol developed by Murphy and Riley [2]. This method was used to measure the free orthoP in the adsorption and hydrolysis studies.

QCM-D. Samples of polyP (50 mg/L, 15 and 60 phosphate units) were combined with sodium chloride solution (0.1 M, pH 6). Solutions were flowed into the modules of the Q-Sense E4 QCM-D containing sensors coated with iron oxide, Fe_2O_3, or aluminum oxide, Al_2O_3.

Enzymatic Hydrolysis. Alkaline phosphatase (0.5 units/mL) was prepared in Tris buffer (0.1M, pH 9) containing $MgCl_2$ (0.005 M). Enzyme solution (9 mL) was combined with polyP (15, 60, and 130P) stock solution to reach a final orthoP concentration of 980 μM. In parallel, $CaCl_2$ (0.5 M, 0.2 mL) was added to separate polyP-enzyme solutions (15 and 130P) to reach a concentration of 10 mM Ca^{2+}. All samples were incubated at 37°C.

Characterization Studies. Nucleation of precipitates during hydrolysis of polyP with calcium was monitored via dynamic light scattering (DLS) using the Malvern nano-ZS zetasizer. Precipitates were characterized alongside amorphous and crystalline hydroxylapatite (HAP), a model Ca-P species, using the LEO1530 SEM-EDX and ThermoScientific Nicolet iS50 FT-IR ATR with diamond crystal (2 cm step, 64 scans per read).

Results:

Transport. QCM-D results showed the real-time adsorption of 15 and 60P polyP onto Fe_2O_3 and Al_2O_3 (Figure 1). It was observed that polyP is capable of adsorbing onto these naturally abundant mineral species, and due to the fairly uniform adsorbed masses despite the different chain lengths, we hypothesized that the polyP adsorbs on its side instead of terminally. The low loss of mass after the reintroduction of a background solution around 2250 seconds also suggests that the adsorption was irreversible.

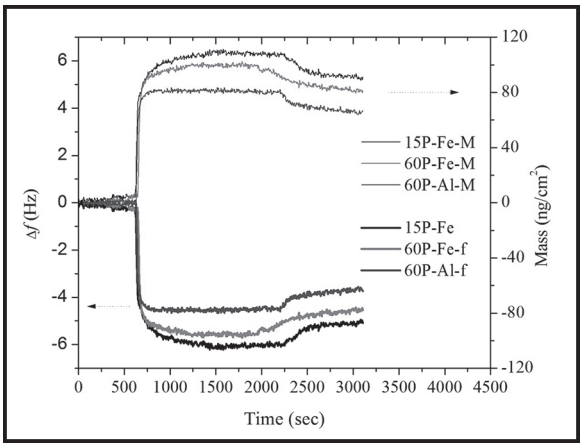

Figure 1: QCM-D monitoring of the adsorption of polyP onto amorphous Al_2O_3 and Fe_2O_3.

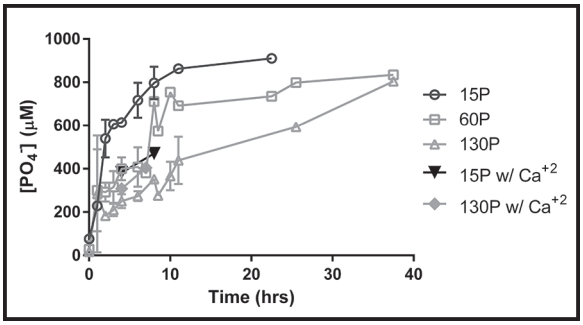

Figure 2: PO_4 produced from APase catalyzed hydrolysis of polyP for varying chain lengths with or without calcium.

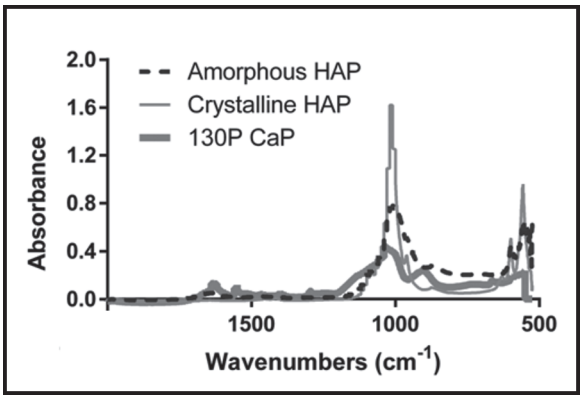

Figure 3: FT-IR spectra of Ca-P and HAP species.

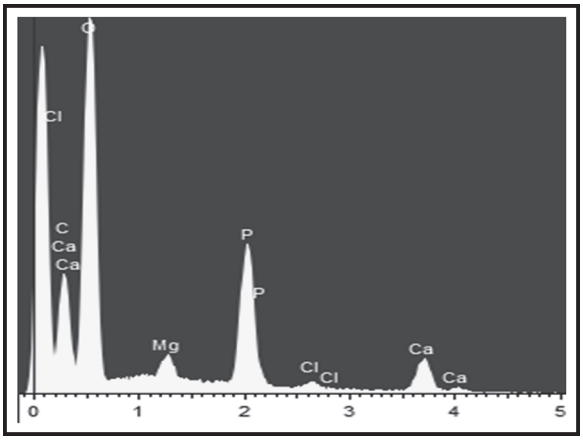

Figure 4: EDX spectrum of Ca-P precipitate.

Transformation. Figure 2 shows orthoP formed over time from different polyP with and without the presence of calcium. Incubation with APase resulted in a faster rate and greater extent of degradation for the shorter polyP compared to that of longer polyP. We believe the hydrolysis was via the terminals of the polyP and followed a consecutive first-order kinetic model. This can be modeled using the equation $[orthoP] = [orthoP]_0 (1\text{-}exp(k_1t))$ [3]. The experimental parameters for hydrolysis of 15, 60, and 130P were 0.2204, 0.1049, and 0.05, respectively.

Mineralization. Precipitation of a possible Ca-P mineral was observed during the hydrolysis of all polyP lengths in the presence of calcium. FT-IR spectra of the observed Ca-P and both amorphous and crystalline HAP is shown in Figure 3. Based on the vibrational mode peaks, we can confirm that the precipitate was some type of Ca-P species. EDX elemental analysis is shown in Figure 4. The observed Ca/P ratio is around 1.0, nearly fitting into the amorphous Ca-P ratio of 1.2 - 2.2. The ratio observed in crystalline HAP is 1.67 [4]. Based on these results, the observed Ca-P was most likely some type of amorphous intermediate phase.

Conclusions and Future Work:

PolyP was found to irreversibly adsorb onto Fe_2O_3 and Al_2O_3, and was hydrolyzed with a rate and extent dependent on chain length. In the presence of calcium and APase, Ca-P precipitates formed. Future work is needed to characterize the effects of more environmentally relevant conditions and different solution chemistries on the behavior of polyP as well as other potential mineralization pathways.

Acknowledgements:

I would like to express my gratitude for the guidance I received from my PI, Yuanzhi Tang, and mentor, Rixiang Huang, as well as the entire Tang group. I would also like to thank the Institute of Electronics and Nanotechnology at the Georgia Institute of Technology, the NNIN REU Program staff, and NSF, Grant No. ECCS-0335765, for making this research possible.

References:

[1] Diaz, J.; Ingall, et al. Science 2008.

[2] Murphy, J., et al. Anal. Chim. Acta. 1962.

[3] Robertson, K. "The Study of Polyphosphate Hydrolysis using 31P NMR." 2015.

[4] Berzina-Cimdina, L., et al. "Infrared Spectroscopy - Materials Science, Engineering and Technology." 2012.

Designing a Conjugated Polymer Consisting of Phenyl-Oxazole Derivatives Using C-H/C-O Coupling

Alin Miksi Kalayjian
Chemistry, University of California, Berkeley

NNIN REU Site: Washington Nanofabrication Facility and Molecular Analysis Facility, University of Washington, Seattle, WA
NNIN REU Principal Investigator: Dr. Christine K. Luscombe, Materials Science and Engineering, University of Washington
NNIN REU Mentor: Jason Lee, Chemistry, University of Washington
Contact: akalayjian@berkeley.edu, luscombe@uw.edu, leejason@uw.edu

Abstract:

Organic π-conjugated semiconducting polymers that have good electronic properties are very important in the development of organic solar cells. Traditionally, organometallic reagents are used in order to perform carbon-carbon coupling reactions of monomers to synthesize conjugated polymers. This requires stoichiometric amounts of organometallic compounds and additional synthetic steps compared to C-H activation chemistry in polymer synthesis. C-H activation eliminates the need to pre-functionalize the normally inert C-H bond found in many organic compounds with metals or other harsher reagents. The C-H activation will reduce byproducts, waste, and inorganic materials, which will aid in the development of "green" reactions. Itami, et al., found that easily synthesized phenol derivatives (containing a C-O-R electrophile) could activate the C-H bond in the 5-position of oxazoles to form a C-C bond [1]. Our work was inspired by this, and the goal of this research was to draw from this methodology to design and synthesize a monomer that had both an electrophilic C-O-R group containing a phenyl ring and an oxazole such that it could undergo polymerization via C-H activation to make a donor-acceptor polymer. Future work includes the study of polymerization growth kinetics and its semiconducting properties.

Introduction:

In recent years, semiconductors have changed the course of human technological advancement. Semiconductors are used in solar cells and in all electronic devices. Silicon (Si) is the most widely used semiconductor. However, making Si based devices is expensive where Si must be extremely pure, which requires energy and time. It also utilizes toxic materials during production that adds more inorganic waste to our environment.

Organic semiconductors, specifically π-conjugated polymers, have been attracting interest as an alternative to Si. Devices made out of organic polymers have advantages over Si based devices because they can be made to be semi-transparent, colorful, and flexible, which give them further range of usage such as in photovoltaics and solar cells. In addition, they require a lower cost of production.

Organic polymer synthesis techniques have developed through the years. However, it has a problem, which is the usage of organometallic reagents (Sn, Li). In order to overcome this issue, C-H activation has been presented as an alternative method to use less organometallic reagents during synthesis. C-H activation utilizes C-H/C-X (X is a halogen) that replaces C-M/C-X (M is metal) in traditional C-C coupling. This eliminates excess transition metal usage creating "green" reactions and less waste product.

The target of this work was to synthesize a π-conjugated polymer by first creating the monomer that is made of phenyl-oxazole derivatives, and by utilizing the C-H/C-O coupling method (inspired by Itami, et al. [1]) polymerize the monomer in order to achieve the conjugated organic semiconducting polymers for its usage in solar cells.

Methodology:

The synthetic steps are shown in Figure 1.

Phenyl-oxazole derivatives are synthesized from the starting material, 2,4-dimethoxy benzaldehyde **1**, which is transformed into first phenyl-oxazole derivative by ring closure **2**. Then, the product is dealkylated to yield the next product **3**, and finally by protection using *p*-toluenesulfonyl group followed by an alkylation, product **5** is obtained.

Results and Discussion:

Analysis of hydrogen nuclear magnetic resonance (^{1}H NMR) data shows that the monomer precursers (phenyl-oxazole derivatives) **2** and **3** were formed (Figure 2). The labeled peaks clearly show that the desired monomer was formed.

In Figure 3, the final monomer synthesis step (protection via *p*-toluensulfonyl group and alkylation by bromohexane) gave mixed results. ^{1}H NMR data showed extra peaks that were not identified. There are extra peaks, d, of tosylate in Figure 3. This may be due to mixed protection where the tosylate reacted at the *ortho* position rather than the *para* position. However, the promising signs are the identification of oxazole peaks a, b, and some aromatic peaks labeled c, g, and f of benzene.

Conclusions:

The synthesis of monomer **5**, consisting of a phenyl-oxazole derivatives, was attempted. The synthesis of the first two precursors proved successful, but the final monomer was not completely synthesized. Oxazole formation by ring closure using toluensulfonylmethyl isocyanide was accomplished. Although the synthesis of the monomer initially was promising, further work needs to be done in order to fully obtain the monomer to perform the synthesis of the desired polymer by utilizing C-H/C-O cross coupling reaction.

Future Work:

So far, the only step that failed was the final step required to fully obtain the desired monomer consisting of phenyl-oxazole derivatives. Therefore, changing the tosylate group with triflate group would be an option. In addition, triflate group would be a better reactive C-O functional group for the polymerization step. If proven to be successful, polymerization will be attempted and further investigation will be done to characterize the polymer such as its growth kinetics and its capacity as a semiconductor for solar cell usage.

Acknowledgments:

I would like to thank Jason Lee for his great help and patience. Thanks to Vicky Pakhnyuk for her help in the lab during my mentor's absence. Most importantly, I would like to thank Dr. Christine K. Luscombe for giving me the opportunity of working in her lab and being part of her interesting research work and group as well as her help with my presentations and papers. Lastly, thank you to the National Nanotechnology Infrastructure Network Research Experience for Undergraduates (NNIN REU) Program and National Science Foundation (NSF) for funding under Grant No. ECCS-0335765.

References:

[1] Muto, K.;Yamaguchi, J.; Itami, K.; Nickel Catalyzed C-H/C-O Coupling of Azoles with Phenol Derivatives. Journal of the American Chemical Society. 2012, 134, 169-172.

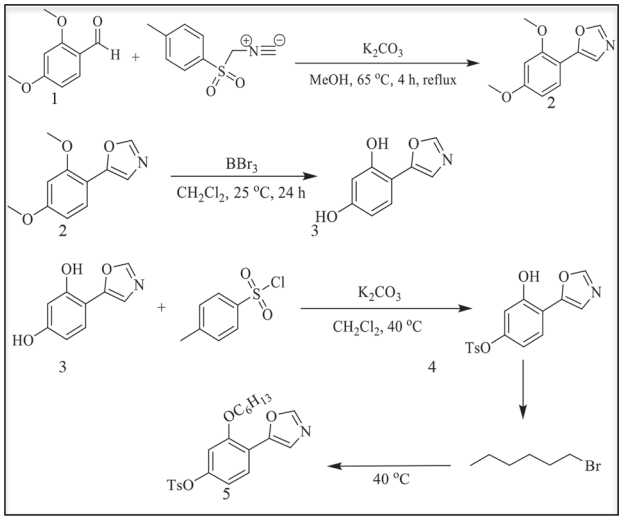

Figure 1: Monomer synthesis scheme in order from top to bottom.

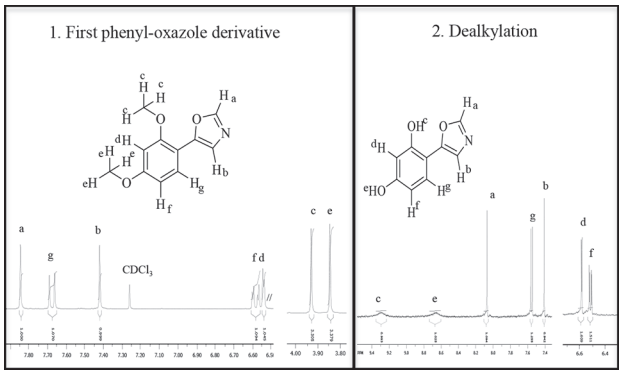

*Figure 2: ^{1}H NMR of molecules **2** and **3**.*

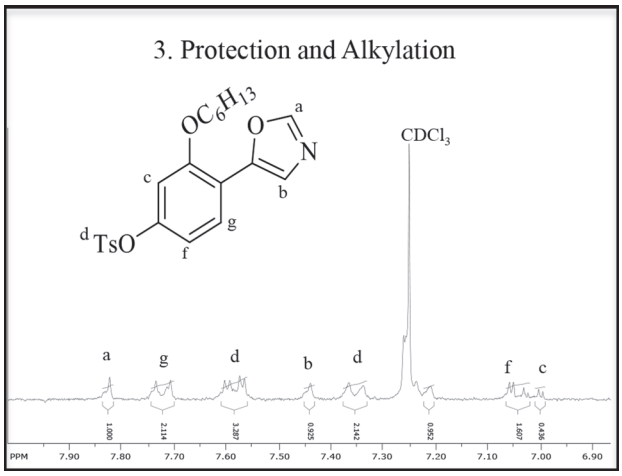

*Figure 3: ^{1}H NMR of product **5** mixture.*